Explosive volcanic eruptions from linear vents on Earth, Venus, and Mars: Comparisons with circular vent eruptions

Lori S. Glaze,[1] Stephen M. Baloga,[2] and Jesse Wimert[3]

Received 25 January 2010; revised 30 September 2010; accepted 5 November 2010; published 28 January 2011.

[1] Conditions required to support buoyant convective plumes are investigated for explosive volcanic eruptions from circular and linear vents on Earth, Venus, and Mars. Vent geometry (linear versus circular) plays a significant role in the ability of an explosive eruption to sustain a buoyant plume. On Earth, linear and circular vent eruptions are both capable of driving buoyant plumes to equivalent maximum rise heights; however, linear vent plumes are more sensitive to vent size. For analogous mass eruption rates, linear vent plumes surpass circular vent plumes in entrainment efficiency approximately when $L_o \geq 3r_o$ owing to the larger entrainment area relative to the control volume. Relative to circular vents, linear vents on Venus favor column collapse and the formation of pyroclastic flows because the range of conditions required to establish and sustain buoyancy is narrow. When buoyancy can be sustained, however, maximum plume heights exceed those from circular vents. For current atmospheric conditions on Mars, linear vent eruptions are capable of injecting volcanic material slightly higher than analogous circular vent eruptions. However, both geometries are more likely to produce pyroclastic fountains, as opposed to convective plumes, owing to the low-density atmosphere. Because of the atmospheric density profile and water content on Earth, explosive eruptions enjoy favorable conditions for producing sustained buoyant columns, while pyroclastic flows would be relatively more prevalent on Venus and Mars. These results have implications for the injection and dispersal of particulates into the planetary atmosphere and the ability to interpret the geologic record of planetary volcanism.

Citation: Glaze, L. S., S. M. Baloga, and J. Wimert (2011), Explosive volcanic eruptions from linear vents on Earth, Venus, and Mars: Comparisons with circular vent eruptions, *J. Geophys. Res.*, *116*, E01011, doi:10.1029/2010JE003577.

1. Introduction

[2] The mechanisms by which ash and volatiles are transported by explosive volcanism on Venus and Mars are important issues that relate to present-day observations of the surface and the evolution of the climate, atmospheric chemistry and subsurface conditions. Advances in understanding the range of magma compositions on Mars [e.g., *Rieder et al.*, 1997; *Bandfield et al.*, 2000] continue to expand notions of the prevalence of extensive explosive volcanism. Detection of elevated SO_2 in the upper atmosphere of Venus [*Esposito*, 1984; *Moore et al.*, 1992; *Robinson et al.*, 1995; *Glaze*, 1999] and diffuse deposits near the summits of some volcanoes [*Campbell and Rogers*, 1994] also seem consistent with explosive volcanism.

[3] There is abundant geologic evidence on both Venus and Mars for large volume volcanic eruptions from long linear vent systems (e.g., Figure 1). Extensive flood volcanism and very long duration fissure eruptions have been conjectured to have played an important role in the formation of many units and features on Mars [e.g., *Greeley and Spudis*, 1981; *Keszthelyi et al.*, 1999; *Greeley et al.*, 2000; *Keszthelyi et al.*, 2006]. It is becoming increasingly evident that this form of volcanism is also important for Venus. Roughly 20% of the large flow fields on Venus originate from fractures (e.g., Figure 1, right) [*Stofan and Smrekar*, 2005], and clearly fall into the flood lava category, with areal extents ranging from 39,000 to 744,000 km^2 [*Magee and Head*, 2001], and thickness estimates ranging from <100 m to 1 km [*Roberts et al.*, 1992; *Lancaster et al.*, 1995]. Terrestrial flood basalt eruptions, such as the Roza eruption of the Columbia River Basalt Group and those associated with the Deccan province, have been responsible for significant volatile degassing with possible impacts on climate [*Thordarson and Self*, 1996; *Self et al.*, 2006]. However, studies that deal with the volcanic contribution of volatiles into planetary atmospheres [*Greeley*, 1987; *Wilson and Mouginis-Mark*, 2001] have given only limited attention to the ability of plumes associated with explosive phases of large effusive eruptions to transport and disperse volatiles and ash.

[4] Buoyant plumes rising above basaltic fissure eruptions on Earth are well documented [e.g., *Thordarson and Self*,

[1]NASA Goddard Space Flight Center, Greenbelt, Maryland, USA.
[2]Proxemy Research, Gaithersburg, Maryland, USA.
[3]Department of Geology, University of Maryland, College Park, Maryland, USA.

Copyright 2011 by the American Geophysical Union.
0148-0227/11/2010JE003577

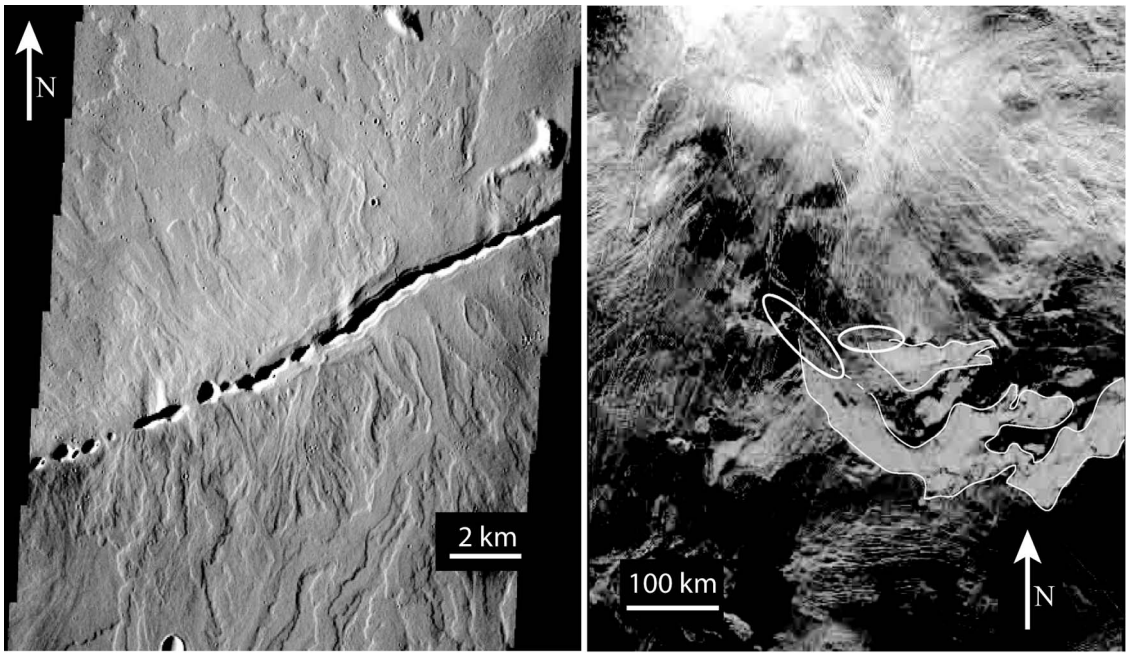

Figure 1. Explosive phases from fissure vents, such as those shown here for (left) Mars (18.1°N 245.3°E; THEMIS visible image V05484014) [*Mouginis-Mark and Christensen*, 2005] and (right) Venus (5.5°S, 206°E, Magellan SAR image), may have contributed significant volatiles to the atmosphere.

1993; *Walker et al.*, 1984; *Lockwood et al.*, 1984; *Thordarson and Larsen*, 2007]. Terrestrial experience [*Thorarinsson*, 1969; *Carracedo et al.*, 1992; *Thordarson and Self*, 1993] indicates that fissure eruptions typically comprise multiple effusive and explosive episodes. These episodes commonly involve localized activity along various subsections of the fissure as the eruption progresses. Active fissure lengths for historical eruptions range from a few hundred meters (e.g., 1961 eruption of Askja, Iceland [*Thorarinsson and Sigvaldason*, 1962], to a few kilometers (e.g., 1886 eruption of Tarawera, New Zealand [*Walker et al.*, 1984], and 1783 eruption of Laki [*Thordarson and Self*, 1993]). The surface expression of fissure vents on Venus and Mars are often tens of km in length. The fissure segment shown in Figure 1 (left) is just part of the overall fissure. Concentric fissures, like those at Alba Patera, are an order of magnitude larger. In addition, volume eruption rates may have been orders of magnitude larger than terrestrial analogs [*Wilson and Mouginis-Mark*, 2001; *Baloga et al.*, 2003; *Baloga and Glaze*, 2008]. Although volcanic fissures visible on the surface of Venus or Mars were not likely active along their entire length at any one time, large conjectured volumetric eruption rates may point to active fissure lengths significantly greater than the documented terrestrial analogs.

[5] Over the last 30 years, there have been numerous models for explosive volcanic eruption columns based on the ideas for buoyant, convecting plumes presented by *Morton et al.* [1956] [e.g., *Wilson*, 1976; *Wilson et al.*, 1978; *Woods*, 1988; *Stothers*, 1989; *Thornhill*, 1993; *Woods*, 1993b; *Glaze et al.*, 1997; *Glaze*, 1999; *Hort and Weitz*, 2001]. However, with the exception of *Stothers* [1989] and *Woods* [1993a], the effects of linear geometry (including multiple aligned point sources) on plume dynamics have largely been ignored. In general, volcanic plume models have focused on eruptions from localized circular vents under the assumption that linear vent plumes that rise much higher than the length of active fissure can be approximated with a point source. The original basis for this assumption was the field work by *Walker et al.* [1984] on the 1886 fissure eruption of Tarawera, the largest historical eruption in New Zealand, where most of the erupted material originated from a series of closely space vents along a 7 km fissure. During its most explosive phase, a Plinian plume rose to an estimated height of 28 km above a 4 km active segment of the fissure. The distal air fall deposit from this Plinian plume exhibits a symmetry consistent with (i.e., indistinguishable from) fallout from a plume originating from a circular vent. *Walker et al.* [1984] infer from the surface distribution of distal ash that, because the rise height was so much greater than the active fissure length, the plume material "forgot" that it originated from an extended source. However, this inference derives from the final surface deposit, and as such, reflects more on the processes that influence settling rather than vertical transport. It ignores the dynamic transport characteristics that might be associated with different vent geometries and the ability of a plume to transport material up to a diffusive regime.

[6] It is not at all unexpected that some component of the fallout deposit from a large linear vent eruption should be more symmetric in nature. First, for narrow linear plumes, most of the entrainment occurs along the linear extent of the plume, and thus expansion perpendicular to the fissure axis is dominant. Expansion parallel to the fissure axis should be small in comparison. Thus, by the time a plume reaches heights such as 28 km, the expansion of the plume may well be more circular in nature. Second, atmospheric diffusion and turbulence during ash fallout [*Suzuki*, 1983; *Armienti et al.*, 1988; *Glaze and Self*, 1991] produce a randomizing effect

Table 1. System of First-Order Partial Differential Equations for Convective Rise, After *Glaze et al.* [1997][a]

Description	Generic Conservation Equation	Central Vent	Linear Vent
Control volume	V	$V = \pi r^2 dz$	$V = 2bLdz$
Entrainment area	A_e	$A_e = 2\pi r dz$	$A_e \approx 2Ldz$
Mass: dry air	$\frac{d}{dz}[\rho_d u V \phi_d] = \rho_a(\alpha u)A_e$	$\frac{d}{dz}[\rho_d u r^2 \phi_d] = 2\alpha\rho_a u r$	$\frac{d}{dz}[\rho_d u b \phi_d] = \alpha\rho_a u$
Mass: vapor	$\frac{d}{dz}[\rho_v u V \phi_v] = 0$	$\frac{d}{dz}[\rho_v u r^2 \phi_v] = 0$	$\frac{d}{dz}[\rho_v u b \phi_v] = 0$
Mass: solid	$\frac{d}{dz}[\rho_s u V \phi_s] = 0$	$\frac{d}{dz}[\rho_s u r^2 \phi_s] = 0$	$\frac{d}{dz}[\rho_s u b \phi_s] = 0$
Mass: bulk	$\frac{d}{dz}[\rho_B u V] = \rho_a(\alpha u)A_e$	$\frac{d}{dz}[\rho_B u r^2] = 2\alpha\rho_a u r$	$\frac{d}{dz}[\rho_B u b] = \alpha\rho_a u$
Momentum	$\frac{d}{dz}[\rho_B u^2 V] = g(\rho_a - \rho_B)V$	$\frac{d}{dz}[\rho_B u^2 r^2] = g(\rho_a - \rho_B)r^2$	$\frac{d}{dz}[\rho_B u^2 b] = g(\rho_a - \rho_B)b$
Energy	$\frac{d}{dz}[\rho_B u V C_B \theta] = \rho_a(\alpha u)C_a\theta_a A_e - \rho_a u g V(\phi_d + \phi_v)$	$\frac{d}{dz}[\rho_B u r^2 C_B \theta] = 2\alpha\rho_a u r C_a\theta_a - \rho_a u r^2 g(\phi_d + \phi_v)$	$\frac{d}{dz}[\rho_B u b C_B \theta] = \alpha\rho_a u C_a\theta_a - \rho_a u g b(\phi_d + \phi_v)$

[a]The control volume and entrainment area can be defined to accommodate either a circular or linear source. See Notation section for definitions.

on the final deposition of ash on the surface, smoothing and masking (i.e., "forgetting") the original linear nature of the plume rise. However, *Walker et al.* [1984] also noted that the thickness of the proximal air fall deposit did not vary much with distance along the 4 km active segment of the fissure. From this observation, they concluded that the entire 4 km fissure segment was likely active concurrently. This observation directly supports the inference that the linear vent geometry is important to the dynamics of the plume transporting the material found in the proximal deposit. Thus, dynamics of plume rise, particularly in the first few kilometers, may be significantly influenced by the vent geometry.

[7] Key issues for planetary explosive volcanism include the heights attainable by convecting plumes, the ability to transport and disperse particulates and volatiles, and the subsurface conditions within the feeding conduit required to sustain a column. All the models based on extensions of the *Morton et al.* [1956] system of equations indicate that atmospheric entrainment in the first few kilometers of the eruption column play a dominant role in the dynamics of buoyant plumes. Entrainment, in turn, depends upon the surface area and upward velocity of the plume in the lower reach.

[8] In this paper, quantitative constraints are developed for the dimensions and character of buoyant columns for a range of active linear and circular vent systems and eruption conditions on the Earth, Venus, and Mars. The influence of atmospheric profile, gravity, geometric and scale differences among these planets are evaluated. This is accomplished by adapting previous models for buoyant plumes arising from central vents [*Glaze and Baloga*, 1996; *Glaze et al.*, 1997; *Glaze*, 1999; *Glaze and Baloga*, 2002] to linear vent geometries. The models used in this work are analogous to the more elementary single-component linear source model of *Stothers et al.* [1986] and *Stothers* [1989] with the adaptation to both solid and vapor plume constituents. The results obtained in this paper provide significant implications for the relative roles of widespread air fall and pyroclastic flow mechanisms in forming the geologic record from explosive volcanism on the terrestrial planets.

2. Convective Plume Model

[9] The approach to modeling linear volcanic vents described here builds on the original work by *Stothers* [1989] but takes advantage of substantial improvements that have been made in volcanic plume modeling over the last 20 years. Changes from the *Stothers* [1989] approach include (1) explicit inclusion of the conservation of thermal energy, as proposed by *Woods* [1988], and implemented by *Glaze and Baloga* [1996], *Glaze et al.* [1997], *Glaze* [1999], and *Glaze and Baloga* [2002], (2) consideration of multiple plume components, particularly solids, and (3) more detailed information on Venus and Mars atmospheric compositions.

[10] In general, the complete system of equations describing buoyant plume rise that must be solved requires at least a half dozen differential equations and another half dozen equations describing parameters within the plume and ambient atmosphere. Table 1 shows the system of differential equations from *Glaze et al.* [1997] where the control volume and entraining area are given in a generic form in the second column (see Notation section for definitions). For the cylindrically axisymmetric system of *Glaze et al.* [1997], shown in Figure 2a, the control volume is defined as $V = \pi r^2 dz$, and the area through which ambient is entrained is $A_e = 2\pi r\ dz$. For the linear vent system shown in Figure 2b, $V = 2bLdz$ and $A_e \approx 2Ldz$ (where it is assumed that $L \gg b$). The approach is then to solve the sets of governing equations in Table 1 for both central and linear vent geometries. The results described below have assumed that L remains relatively constant as a function of z. Thus L does not appear in any of the linear vent conservation equations in Table 1.

[11] Boundary conditions at the vent for all variables (r, b, u, θ, and n) are denoted by a subscripted "o." The vent is defined as the top of the feeding conduit, and the point at which the erupted material is free to entrain ambient atmosphere and expand. Note that the dimensions at the top of the conduit can be considerably smaller than the visible expression of the vent at the surface for both circular and linear vents. Values for the entrainment constant, α, have been estimated for buoyant plumes originating from both circular and linear vents using empirical [e.g., *Batchelor*, 1954; *Morton et al.*, 1956], theoretical [*Agrawal and Prasad*, 2003], and simulation [*Suzuki and Koyaguchi*, 2010] approaches. Values for circular vent plumes range from 0.05–0.15, and from 0.0975–0.16 for linear vent plumes. For the purpose of comparing the effects of geometry only, this study assumes a value of $\alpha = 0.09$ for all cases.

[12] In addition to the conservation equations defined in Table 1, the system is completed by the following definitions: Volume fraction

$$\phi_d + \phi_v + \phi_s = 1 \tag{1}$$

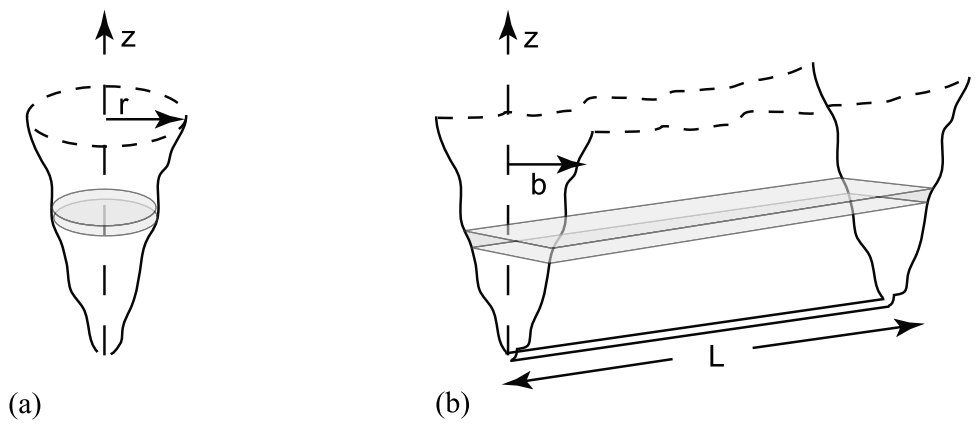

Figure 2. Schematic views of (a) circular and (b) linear vent geometries. The control volume for each plume is indicated by the gray shaded volume. The entrainment area is the outer, exposed surface area of the control volume. The volcanic vent in both cases is defined as the top of the conduit. Boundary conditions at the vent are denoted by variables with "o" subscript. Note that for linear vents, $L_o \gg b_o$, and that L does not change substantially as a function of z.

Ideal gas law

$$P = (\rho_d \phi_d R_d + \rho_v \phi_v R_v)\theta \tag{2}$$

Bulk density

$$\rho_B = \rho_d \phi_d + \rho_v \phi_v + \rho_s \phi_s \tag{3}$$

Bulk specific heat

$$C_B = [\rho_d \phi_d C_a + \rho_v \phi_v C_v + \rho_s \phi_s C_s]/\rho_B \tag{4}$$

[13] Following *Glaze and Baloga* [1996], *Glaze et al.* [1997], *Glaze* [1999], and *Glaze and Baloga* [2002], the systems of ordinary differential equations in Table 1 are solved simultaneously using a Runge-Kutta technique. To avoid numerical artifacts in the boundary region near the plume top, the maximum plume height is defined as the height at which the upward velocity drops to below 10 m s^{-1}. Plume rise beyond this point is minimal (relative to the overall plume height), while the velocity drops quickly and the corresponding plume radius (or half width for linear plumes) increases exponentially.

3. Results for Earth's Atmosphere

[14] Much has been published on the sensitivities of the central vent model given in Table 1 [e.g., *Wilson*, 1976; *Wilson et al.*, 1978; *Woods*, 1988; *Glaze and Baloga*, 1996; *Glaze et al.*, 1997]. Thus, here, the focus is on the primary differences that result from the linear vent geometry relative to the central vent. The numerical code used to solve the linear vent system is identical to the central vent model, where the only differences are those resulting from the geometry of the vents.

[15] Figure 3 illustrates a basic comparison of predicted plume heights on Earth for a range of vent sizes. As noted above, the length of fissure vent that is active does not appear in the conservation equations in Table 1. Thus, a simple comparison can be made of plume height as a function of either b_o (for linear vents) or r_o (for circular vents). For the results shown in Figure 3, all of the boundary values at the vent are kept the same, except for the size of the vent opening (radius, r_o, for circular vents, or half width, b_o, for linear vents). The vent conditions used for both geometries are velocity, u_o = 300 m s^{-1}, temperature, θ_o = 1000 K, and the mass fraction of water vapor, n_o = 0.03, where the mass fraction of vapor in the plume is defined as $n = \rho_v \phi_v / \rho_B$. For this example, the plumes are assumed to rise from sea level into the U.S. Standard Atmosphere [e.g., *Wallace and Hobbs*, 1977].

[16] For this set of boundary conditions both the linear and circular vent models produce a maximum plume height of around 35 km. Figure 3 shows maximum plume heights for circular and linear vents, plotted for a broad range of vent sizes. From this plot, it can be seen that buoyant, convecting plumes originating from circular vents can be maintained with substantial maximum heights over a wide range of vent

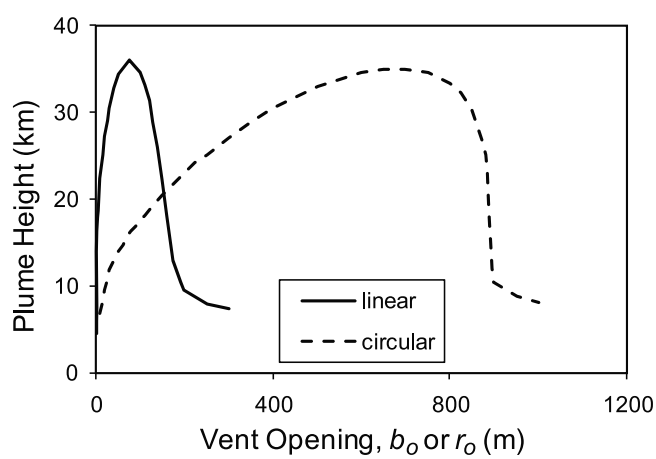

Figure 3. Maximum predicted plume heights as a function of either vent radius (for circular vents), r_o, or half width (for linear vents), b_o. Models assume terrestrial ambient atmospheric conditions with temperature and pressured defined by the U.S. Standard Atmosphere, u_o = 300 m s^{-1}, θ_o = 1000 K, and n_o = 0.03.

Table 2. Comparison of Terrestrial Vent Sizes for Circular and Linear Vents and a Range of Cross-Sectional Vent Areas

		b_o (m)					
A_o (m^2)	r_o (m)	L_o = 500 m	L_o = 1000 m	L_o = 2000 m	L_o = 3000 m	L_o = 5000 m	L_o = 10000 m
3.14×10^2	10	0.314	0.157	0.079	0.052	0.031	0.016
1.96×10^3	25	1.96	0.982	0.491	0.327	0.196	0.098
6.36×10^3	45	6.36	3.18	1.59	1.06	0.636	0.318
1.54×10^4	70	15.4	7.70	3.85	2.57	1.54	0.770
7.07×10^4	150	-	35.3	17.7	11.8	7.07	3.53
1.52×10^5	220	-	76.0	38.0	25.3	15.2	7.60
2.83×10^5	300	-	-	70.7	47.1	18.3	14.1
5.03×10^5	400	-	-	126	83.8	50.3	25.1
7.85×10^5	500	-	-	196	131	78.5	39.3
1.65×10^6	725	-	-	-	275	165	82.6
2.46×10^6	885	-	-	-	-	246	123
3.14×10^6	1000	-	-	-	-	314	157

sizes, from a radius of a few meters to around 900 m. For the boundary conditions used in this analysis, plumes from circular vents collapse, or are otherwise unable to maintain a steady column, for vent sizes greater than about 900 m. However, the linear plumes are much more sensitive to the vent size, and can maintain a convective plume over a much more narrow range of vent sizes. For the same boundary conditions (temperature, velocity, gas mass fraction), plumes from linear vents only reach significant heights for values of b_o of a few meters to ~200 m. For this set of boundary conditions, the peak plume height occurs when $b_o \approx 75$ m.

[17] Because one of the main drivers of plume height is the mass flux at the vent [*Woods*, 1988; *Glaze and Baloga*, 1996], a better comparison between linear and circular vents can be made by examining predicted plume heights for equivalent mass fluxes. The mass flux at the vent is defined as the density of the erupted material multiplied by the cross-sectional area of the vent and the exit velocity ($= \rho_{Bo} u_o A_o$). Keeping the bulk plume density and exit velocities the same for both linear and circular vents, the key parameter for comparison becomes the cross-sectional vent area, where $A_o = \pi r_o^2$ for the circular vent, and $A_o = 2b_o L_o$ for the linear vent.

[18] Column 1 of Table 2 indicates a range of cross-sectional vent areas. Column 2 of Table 2 contains the corresponding radii for circular vents. For linear vents, the half width b_o, corresponding to the cross-sectional area is dependent upon the choice for active fissure length, L_o. Noting that the original definition of a linear vent included the assumption that $L_o \gg b_o$, Table 2 only considers values for b_o that are less than an order of magnitude smaller than L_o. Active fissure lengths up to 10 km are considered.

[19] Figure 4 illustrates the plume heights corresponding to the vent sizes given in Table 2. From Figure 4, it can be seen that as L_o increases, linear plumes become more capable of establishing a convective regime over a broad range of b_o, similar to the circular vents. This is primarily because as L_o increases, the entrainment area of the linear plumes increases relative to the control volume. The ability of a plume to become buoyant is driven by whether or not sufficient air can be entrained (and warmed) to reduce the bulk plume density before upward momentum is exhausted. From the right-hand side of the dry air mass conservation equations in Table 1, the mass of dry air entrained by the linear plume is roughly the same as the cylindrical case when $uL \approx \pi ur$. Thus, the linear plumes surpass circular vents in entrainment efficiency approximately when $L_o \geq 3r_o$. Note, however, that because L does not appear in the governing equations, the maximum plume height in Figure 4 always occurs around $b_o \approx 75$ m.

4. Applications to Venus and Mars

[20] Analysis of the linear vent model under ambient conditions found on Venus and Mars are now considered.

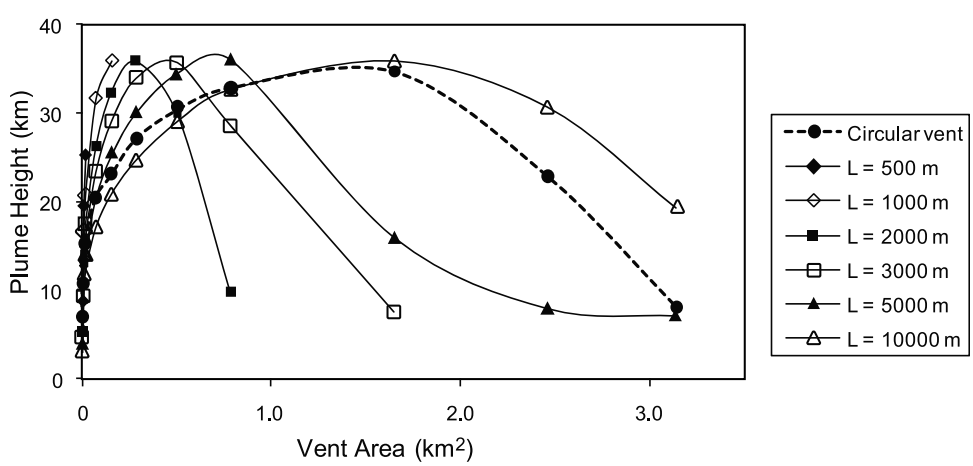

Figure 4. Maximum predicted plume heights as a function of vent area. Model boundary conditions are the same as those in Figure 3. The linear vent results are shown for multiple choices of active fissure length.

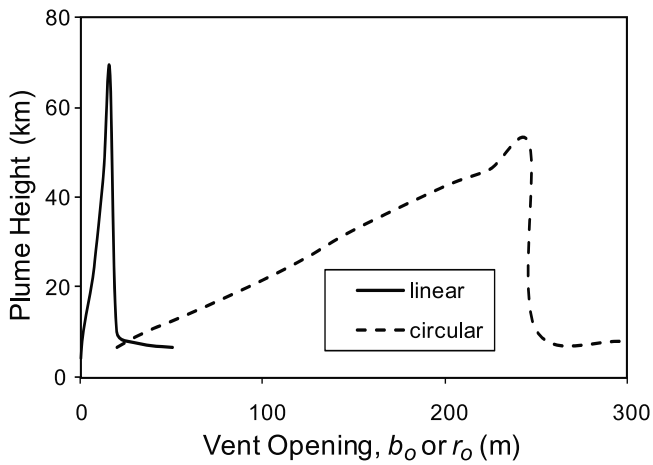

Figure 5. Maximum predicted plume heights on Venus as a function of either vent radius (for circular vents), r_o, or half width (for linear vents), b_o. Models assume northern Venus latitude ambient atmospheric conditions, u_o = 270 m s^{-1}, θ_o = 1400 K, and n_o = 0.05.

Because of the extreme differences in the atmospheric densities, boundary condition values used in these analyses are slightly different than those used for Earth.

[21] For comparison with conditions considered by *Glaze* [1999], the variables held constant under Venus conditions are the initial velocity, u_o = 270 m s^{-1}, initial temperature, θ_o = 1400 K, and the mass fraction of water vapor, n_o = 0.05. Further, the scenarios discussed here have used the high-latitude atmospheric temperature and pressure profile [*Seiff et al.*, 1985], as explosive eruptions under these conditions were shown by *Glaze* [1999] to be the most likely to rise to significant altitudes. The primary difference between the boundary conditions used here and those used by *Glaze* [1999] is that here it has been assumed that the vent is at 0 km above the mean planetary radius (as opposed to 10 km ampr).

[22] Figure 5 shows the plume heights reached for circular and linear vents for a range of radii and half widths, respectively. There are several points of interest to note. First, consistent with work by *Thornhill* [1993] and *Glaze* [1999], the range of conditions over which buoyant plumes can be maintained on Venus is very narrow (note the range on the x axis is only 300 m, compared to >800 m on Earth). Also, the shape of the curve for circular vents is substantially different from the terrestrial case, with an almost linear relationship between vent radius and maximum plume height. The primary explanation for this difference in shape is the much higher-pressure ambient atmosphere.

[23] The maximum plume height achievable for the given boundary conditions is ~52 km corresponding to a circular vent radius of 247 m. Like the terrestrial case, there is a very abrupt break at the point where a convective plume can no longer be maintained. For linear vents, the range of conditions that can maintain a convective plume is likewise very narrow, with the maximum plume height of ~69 km occurring when b_o = 16 m. Unlike the terrestrial case, linear vents on Venus appear capable of driving a plume to somewhat higher maximum altitudes, for all other things remaining equal, albeit under very limited conditions.

[24] As for Earth, a better comparison between the circular and linear vents is made by looking at the plume heights for each when the mass flux at the vent (and thus the cross-sectional vent area) is the same. Table 3 indicates circular vent radii and linear vent half widths for a range of cross-sectional vent areas. Again, the linear vent half widths are restricted to those that are less than an order of magnitude smaller than the fissure length, consistent with the assumption that $b_o \ll L_o$.

[25] Figure 6 shows the predicted plume heights for the vent sizes given in Table 3. It can be seen that the maximum plume height for the linear vent case occurs consistently for b_o = 16 m, but the peak is shifted to the right by increasing the active fissure length (i.e., L). Unlike the terrestrial example, however, the linear vent is more effective than its circular counterpart at producing a convective plume that is capable of reaching significant heights for the same mass flux.

[26] For Mars, the variables held constant are initial velocity, u_o = 230 m s^{-1}, initial temperature, θ_o = 1000 K, and mass fraction of water vapor, n_o = 0.01. It should be noted that *Glaze and Baloga* [2002] placed limits on the applicability of buoyancy models such as the one described here. That study indicated that such models are not valid above heights greater than 10–20 km on Mars under current atmospheric conditions. For those boundary conditions that produce plumes higher than about 10 km, the alternative approach of *Wilson and Head* [2007] is used to model the subsequent inertial transport of particles along ballistic trajectories. Using this

Table 3. Comparison of Volcanic Vent Sizes on Venus for Circular and Linear Vents and a Range of Cross-Sectional Vent Areas

		b_o (m)				
A_o (m^2)	r_o (m)	L_o = 200 m	L_o = 500 m	L_o = 1000 m	L_o = 2000 m	L_o = 5000 m
1.26 × 10^3	20	3.14	1.26	0.628	0.314	0.126
2.83 x 103	30	7.07	2.83	1.41	0.707	0.283
7.85 × 10^3	50	19.6	7.85	3.93	1.96	0.785
1.54 × 10^4	70	-	15.4	7.69	3.85	1.54
3.13 × 10^4	100	-	31.4	15.7	7.85	3.14
4.90 × 10^4	125	-	49.1	24.5	12.3	4.91
7.07 × 10^4	150	-	-	35.3	17.7	7.07
1.26 × 10^5	200	-	-	62.8	31.4	12.6
1.59 × 10^5	225	-	-	79.5	39.8	15.9
1.96 × 10^5	250	-	-	95.2	49.1	19.6
2.83 × 10^5	300	-	-	-	70.7	28.3

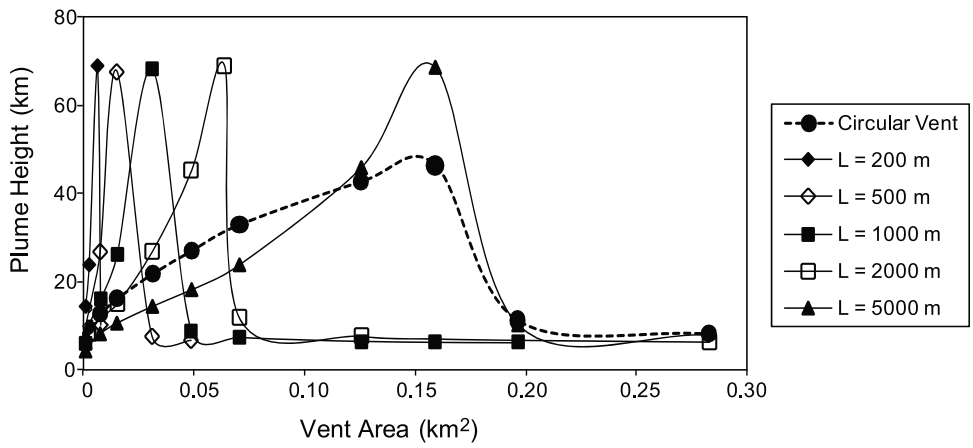

Figure 6. Maximum predicted plume heights on Venus as a function of vent area. Model boundary conditions are the same as those in Figure 5. The linear vent results are shown for multiple choices of active fissure length.

approach, the upward velocity and plume dimensions at 10 km are used as starting conditions for momentum driven rise. Plume heights found using the convective model are compared to the heights found using the combined buoyancy-ballistic approach for the circular and linear vents in Figure 7.

[27] Using the combined buoyancy-ballistic approach, a comparison of the linear and circular vents is made by examining plume heights for fixed mass fluxes (Table 4 and Figure 8), as was done for Earth and Venus. The ballistic constraint above 10 km results in no plumes that rise above 15 km above the vent. The plumes from circular vents decrease in height as the mass flux (i.e., vent area) increases, implying column collapse conditions. However, in contrast, the linear vent plumes continue to show an increase in maximum plume height as mass flux increases, indicating that the upward velocity of the bulk plume material at 10 km altitude (where transport transitions from convective to ballistic) is also increasing. The implication is, therefore, that these linear vent plumes are not necessarily collapsing, and that linear vent plumes develop a pyroclastic fountain capable of injecting a substantial amount of ash and volatiles into the atmosphere at the plume top.

[28] The preference for the formation of pyroclastic flows and near vent deposition on Mars, as opposed to widely dispersed air fall deposits, is consistent with some prior suggestions in the literature. Most notably, interpretations of early volcanic activity [e.g., *Mouginis-Mark et al.*, 1988; *Carr*, 2007] have suggested numerous and extensive pyroclastic flows on the flanks of Alba Patera prior to a transition of late-stage effusive volcanism. Similar considerations may apply to incised units thought to be either air fall or pyroclastic flow deposits at Hecates tholus and Hadriaca and

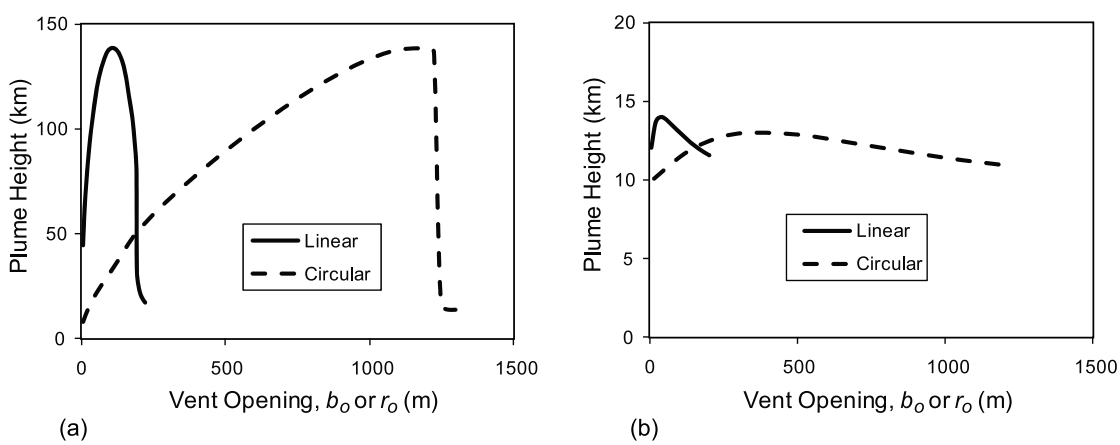

Figure 7. Maximum predicted plume heights on Mars as a function of either vent radius (for circular vents), r_o, or half width (for linear vents), b_o. Models assume the current low-pressure ambient atmospheric conditions, u_o = 230 m s^{-1}, θ_o = 1000 K, and n_o = 0.01. (a) Predicted plume heights for circular and linear vents when convective model is allowed to run to its full extent, regardless of inconsistencies and nonphysical effects (e.g., expansion rates that exceed the speed of sound). (b) Predicted heights for circular and linear vents when convective model is terminated at 10 km. Upward velocity at 10 km is then used to estimate the maximum height for a purely ballistic vertical trajectory.

Table 4. Comparison of Volcanic Vent Sizes on Mars for Circular and Linear Vents and a Range of Cross-Sectional Vent Areas

		b_o (m)				
A_o (m^2)	r_o (m)	L_o = 200 m	L_o = 500 m	L_o = 1000 m	L_o = 2000 m	L_o = 5000 m
849	30	2.12	0.849	0.424	0.212	0.085
3150	100	7.89	3.15	1.57	0.789	0.315
7150	175	17.9	7.15	3.57	1.79	0.715
13700	300	-	13.7	6.83	3.42	1.37
25100	500	-	25.1	12.5	6.27	2.51
37800	700	-	37.8	18.9	9.45	3.78
55700	1000	-	-	27.8	13.9	5.57
59900	1200	-	-	30.0	15.0	5.99

Tyrrhena paterae [*Mouginis-Mark et al.*, 1982; *Greeley and Crown*, 1990; *Gregg and Farley*, 2006].

5. Conclusions

[29] When buoyancy can be sustained, plumes from both linear and circular volcanic vents have very similar maximum heights. However, the conditions required to sustain buoyant plumes are highly restricted for linear vents. The range of conditions for sustained buoyancy is very narrow for Venus and relatively more favorable for the Earth. The dependence of maximum plume height on circular vent diameter is dominated by the nature of the ambient atmospheric profiles for density, pressure, and water content. On Venus, the extreme ambient atmospheric pressures (100 times Earth) result in an almost linear relationship between the vent radius and plume height.

[30] When buoyancy is sustained, linear vents appear to be equally capable of injecting volcanic ash and volatiles into the atmosphere. For analogous mass flux rates at the vent, the maximum heights to which linear and cylindrical plumes can rise are essentially equivalent. In cases where the length of active linear vent is less than approximately $3r_o$, the entrainment area of linear plumes is significantly less than the cylindrical (circular vent) equivalent. Thus the range of vent widths that can sustain a buoyant plume is narrow and these plumes are more likely to collapse.

[31] Only the Earth, with its thick wet atmosphere, favors explosive eruptions that can maintain convective plumes reaching tens of km in altitude. Conversely, the range of plausible conditions that can produce a buoyant convective plume on Venus is very restricted. The probability of an eruption occurring with just the right boundary conditions is relatively small. Thus, it seems that pyroclastic flows are much more likely in the nonterrestrial environments. On Mars, the results presented here favor interpretations of pyroclastic flows and near vent deposition at major volcanic centers, including Alba, Hadriaca, and Tyrrhena paterae and Hecates tholus, where the discriminating morphologic diagnostics remain ambiguous.

Notation

A_o Cross-sectional vent area at the top of the conduit ("o" subscript indicates a value at the vent, defined as the top of the conduit) (m^2).
A_e Entrainment area (m^2).
b Linear plume half width (m).
C_a Specific heat of ambient atmosphere (Earth, 998 J K^{-1} kg^{-1}; Venus and Mars, 835 J K^{-1} kg^{-1}).
C_B Bulk specific heat of plume (J K^{-1} kg^{-1}).
C_v Specific heat of water vapor (= 2000 J K^{-1} kg^{-1}).
C_s Specific heat of solid particles (= 920 J K^{-1} kg^{-1}).

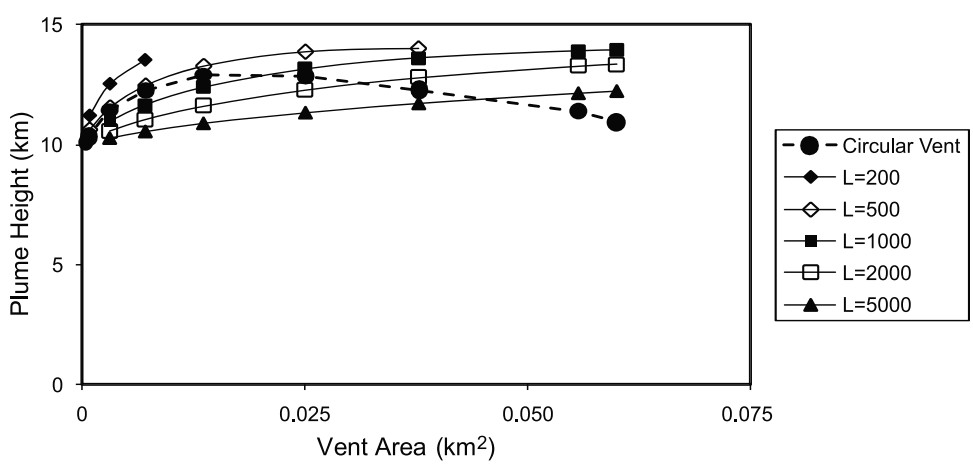

Figure 8. Maximum predicted plume heights on Mars as a function of vent area. Model boundary conditions are the same as those in Figure 7. The convective model has been terminated at 10 km (as in Figure 7b) and subsequent rise determined from a ballistic vertical trajectory. The linear vent results are shown for multiple choices of active fissure length.

g Gravitational constant (Earth, 9.8 m s^{-2}; Venus, 8.4 m s^{-2}; Mars, 3.7 m s^{-2}).
L Fissure length (m).
n Gas mass fraction (= $\rho_v\phi_v/\rho_B$).
P Pressure (Pa).
r Cylindrical plume radius (m).
R_d Gas constant for ambient atmosphere (Earth, 287 J K^{-1} kg^{-1}; Venus and Mars, 191 J K^{-1} kg^{-1}).
R_v Gas constant for water vapor (= 461 J K^{-1} kg^{-1}).
u Bulk rise velocity (m s^{-1}).
V Control volume (m^3).
z Vertical distance (m).
α Entrainment constant (= 0.09).
θ Bulk plume temperature (K).
θ_a Ambient atmosphere temperature (K).
ρ_a Ambient atmospheric density (kg m^{-3}).
ρ_B Bulk plume density (kg m^{-3}).
ρ_d Density of entrained dry air (kg m^{-3}).
ρ_v Density of water vapor (kg m^{-3}).
ρ_s Density of solid particles (= 1000 kg m^{-3}).
ϕ_d Volume fraction of entrained dry air.
ϕ_s Volume fraction of solid particles.
ϕ_v Volume fraction of water vapor.

[32] **Acknowledgments.** This work was funded by the NASA Planetary Geology and Geophysics Program (WBS 811073.02.01.04.44 for L. Glaze, and grant NNX08AF16G for S. Baloga). J. Wimert was supported by L. Glaze (Planetary Geology and Geophysics WBS) through the University of Maryland CRESST program. The authors would like to thank Steve Self for a very constructive review of this manuscript.

References

Agrawal, A., and A. K. Prasad (2003), Integral solution for the mean flow profiles of turbulent jets, plumes and wakes, *J. Fluids Eng.*, *125*, 813–822, doi:10.1115/1.1603303.

Armienti, P., G. Macedonio, and M. T. Pareschi (1988), A numerical model for simulation of tephra transport and deposition; applications to May 18, 1980, Mount St. Helens eruption, *J. Geophys. Res.*, *93*(B6), 6463–6476, doi:10.1029/JB093iB06p06463.

Baloga, S. M., and L. S. Glaze (2008), A self-replication model for long channelized lava flows on the Mars plains, *J. Geophys. Res.*, *113*, E05003, doi:10.1029/2007JE002954.

Baloga, S. M., P. J. Mouginis-Mark, and L. S. Glaze (2003), Rheology of a long lava flow at Pavonis Mons, Mars, *J. Geophys. Res.*, *108*(E7), 5066, doi:10.1029/2002JE001981.

Bandfield, J. L., V. E. Hamilton, and P. R. Christensen (2000), A global view of Martian surface compositions from MGS-TES, *Science*, *287*, 1626–1630, doi:10.1126/science.287.5458.1626.

Batchelor, G. K. (1954), Heat convection and buoyancy effects in fluids, *Q. J. R. Meteorol. Soc.*, *80*, 339–358, doi:10.1002/qj.49708034504.

Campbell, B. A., and P. G. Rogers (1994), Bell Regio, Venus: Integration of remote sensing data and terrestrial analogs for geologic analysis, *J. Geophys. Res.*, *99*(E10), 21,153–21,171, doi:10.1029/94JE01862.

Carr, M. H. (2007), *The Surface of Mars*, 322 pp., Cambridge Univ. Press, Cambridge, U. K.

Carracedo, J. C., E. Rodriguez Badiola, and V. Soler (1992), The 1730–1736 eruption of Lanzarote, Canary Islands: A long, high-magnitude basaltic fissure eruption, *J. Volcanol. Geotherm. Res.*, *53*, 239–250, doi:10.1016/0377-0273(92)90084-Q.

Esposito, L. W. (1984), Sulfur dioxide: Episodic injection shows evidence for active Venus volcanism, *Science*, *223*, 1072–1074, doi:10.1126/science.223.4640.1072.

Glaze, L. S. (1999), Transport of SO_2 by explosive volcanism on Venus, *J. Geophys. Res.*, *104*(E8), 18,899–18,906, doi:10.1029/1998JE000619.

Glaze, L. S., and S. M. Baloga (1996), Sensitivity of buoyant plume heights to ambient atmospheric conditions: Implications for volcanic eruption columns, *J. Geophys. Res.*, *101*(D1), 1529–1540, doi:10.1029/95JD03071.

Glaze, L. S., and S. M. Baloga (2002), Volcanic plume heights on Mars: Limits of validity for convective models, *J. Geophys. Res.*, *107*(E10), 5086, doi:10.1029/2001JE001830.

Glaze, L. S., and S. Self (1991), Ashfall dispersal for the 16 September 1986, eruption of Lascar, Chile, calculated by a turbulent diffusion model, *Geophys. Res. Lett.*, *18*(7), 1237–1240, doi:10.1029/91GL01501.

Glaze, L., S. M. Baloga, and L. Wilson (1997), Transport of atmospheric water vapor by volcanic eruption columns, *J. Geophys. Res.*, *102*(D5), 6099–6108, doi:10.1029/96JD03125.

Greeley, R. (1987), Release of juvenile water on Mars: Estimated amounts and timing associated with volcanism, *Science*, *236*, 1653–1654, doi:10.1126/science.236.4809.1653.

Greeley, R., and D. Crown (1990), Volcanic geology of Tyrrhena Patera, Mars, *J. Geophys. Res.*, *95*(B5), 7133–7149, doi:10.1029/JB095iB05p07133.

Greeley, R., and P. D. Spudis (1981), Volcanism on Mars, *Rev. Geophys.*, *19*(1), 13–41, doi:10.1029/RG019i001p00013.

Greeley, R., N. T. Bridges, D. A. Crown, L. S. Crumpler, S. A. Fagents, P. J. Mouginis-Mark, and J. Zimbelman (2000), Volcanism on the Red Planet: Mars, in *Environmental Effects on Volcanic Eruptions: From Deep Oceans to Deep Space*, edited by J. Zimbelman and T. K. P. Gregg, pp. 75–112, Kluwer Acad., New York.

Gregg, T. K. P., and M. A. Farley (2006), Mafic pyroclastic flows at Tyrrhena Patera, Mars: Constraints from observations and models, *J. Volcanol. Geotherm. Res.*, *155*, 81–89, doi:10.1016/j.jvolgeores.2006.02.008.

Hort, M., and C. M. Weitz (2001), Theoretical modeling of eruption plumes on Mars under current and past climates, *J. Geophys. Res.*, *106*(E9), 20,547–20,562, doi:10.1029/2000JE001293.

Keszthelyi, L., S. Self, and T. Thordarson (1999), Application of recent studies on the emplacement of basaltic lava flows to the Deccan Traps, *Mem. Geol. Soc. India*, *43*, 485–520.

Keszthelyi, L., S. Self, and T. Thordarson (2006), Flood lavas on Earth, Io and Mars, *J. Geol. Soc.*, *163*, 253–264, doi:10.1144/0016-764904-503.

Lancaster, M., J. E. Guest, and K. P. Magee (1995), Great lava flow fields on Venus, *Icarus*, *118*, 69–86, doi:10.1006/icar.1995.1178.

Lockwood, J. P., et al. (1984), Mauna Loa Volcano, Hawaii, *Sci. Event Alert Network Bull.*, *03/1984*, Smithsonian Institution, Washington, D. C.

Magee, K., and J. W. Head (2001), Large flow fields on Venus: Implications for plumes, rift associations, and resurfacing, *Spec. Pap. Geol. Soc. Am.*, *352*, 81–101.

Moore, H. J., J. J. Plaut, P. M. Schenk, and J. W. Head (1992), An unusual volcano on Venus, *J. Geophys. Res.*, *97*(E8), 13,479–13,493, doi:10.1029/92JE00957.

Morton, B. R., S. G. Taylor, and J. S. Turner (1956), Turbulent gravitational convection from maintained and instantaneous sources, *Proc. R. Soc. A*, *234*, 1–23.

Mouginis-Mark, P. J., and P. R. Christensen (2005), New observations of volcanic features on Mars from the THEMIS instrument, *J. Geophys. Res.*, *110*, E08007, doi:10.1029/2005JE002421.

Mouginis-Mark, P., L. Wilson, and J. Head III (1982), Explosive volcanism on Hecates Tholus, Mars: Investigation of eruption conditions, *J. Geophys. Res.*, *87*(B12), 9890–9904, doi:10.1029/JB087iB12p09890.

Mouginis-Mark, P. J., L. Wilson, and J. Zimbelman (1988), Polygenic eruptions on Alba Patera, Mars, *Bull. Volcanol.*, *50*(6), 361–379, doi:10.1007/BF01050636.

Rieder, R., T. Economou, H. Wanke, A. Turkevich, J. A. Crisp, J. Bruckner, G. Dreibus, and H. Y. McSween (1997), The chemical composition of Martian soil and rocks returned by the mobile Alpha Proton X-ray Spectrometer: Preliminary results from the X-ray mode, *Science*, *278*, 1771–1774, doi:10.1126/science.278.5344.1771.

Roberts, K. M., J. E. Guest, J. W. Head, and M. G. Lancaster (1992), Mylitta Fluctus, Venus: Rift-related centralized volcanism and the emplacement of large-volume flow units, *J. Geophys. Res.*, *97*, 15,991–16,015, doi:10.1029/92JE01245.

Robinson, C. A., G. D. Thornhill, and E. Parfitt (1995), Large-scale volcanic activity at Maat Mons: Can this explain fluctuations in atmospheric chemistry observed by Pioneer Venus?, *J. Geophys. Res.*, *100*(E6), 11,755–11,763, doi:10.1029/95JE00147.

Seiff, A., J. T. Schofield, A. J. Kliore, F. W. Taylor, S. S. Limaye, H. E. Revercomb, L. A. Sromovsky, V. V. Kerzhanovich, V. I. Moroz, and M. Y. Marov (1985), Models of the structure of the atmosphere of Venus from the surface to 100 kilometers altitude, *Adv. Space Res.*, *5*(11), 3–58, doi:10.1016/0273-1177(85)90197-8.

Self, S., M. Widdowson, T. Thordarson, and A. E. Jay (2006), Volatile fluxes during flood basalt eruptions and potential effects on the global environment: A Deccan perspective, *Earth Planet. Sci. Lett.*, *248*, 518–532, doi:10.1016/j.epsl.2006.05.041.

Stofan, E. R., and S. E. Smrekar (2005), Large topographic rises, coronae, large flow fields and large volcanoes on Venus: Evidence for mantle plumes?, in *Mantle Plume IV Penrose Conference*, *Spec. Publ. Geol. Soc. Am.*, 388, 841–861.

Stothers, R. B. (1989), Turbulent atmospheric plumes above line sources with an application to volcanic fissure eruptions on the terrestrial planets, *J. Atmos. Sci.*, *46*(17), 2662–2670, doi:10.1175/1520-0469(1989)046<2662:TAPALS>2.0.CO;2.

Stothers, R. B., J. Wolff, S. Self, and M. R. Rampino (1986), Basaltic fissure eruption plume heights and atmospheric aerosols, *Geophys. Res. Lett.*, *13*(8), 725–728, doi:10.1029/GL013i008p00725.

Suzuki, T. (1983), A theoretical model for dispersion of tephra, in *Arc Volcanism: Physics and Tectonics*, edited by D. Shimozuru and I. Yokoyama, pp. 95–113, Terra Sci., Tokyo.

Suzuki, Y. J., and T. Koyaguchi (2010), Numerical determination of the efficiency of entrainment in volcanic eruption columns, *Geophys. Res. Lett.*, *37*, L05302, doi:10.1029/2009GL042159.

Thorarinsson, S. (1969), The Laki eruption of 1783, *Bull. Volcanol.*, *33*, 910–929, doi:10.1007/BF02596756.

Thorarinsson, S., and G. E. Sigvaldason (1962), The eruption of Askja 1962: A preliminary rerpot, *Am. J. Sci.*, *260*, 641–651, doi:10.2475/ajs.260.9.641.

Thordarson, T., and G. Larsen (2007), Volcanism in Iceland in historical time: Volcano types, eruption styles and eruptive history, *J. Geodyn.*, *43*, 118–152, doi:10.1016/j.jog.2006.09.005.

Thordarson, T., and S. Self (1993), The Laki (Skaftár Fires) and Grímsvötn eruptions in 1783–1785, *Bull. Volcanol.*, *55*, 233–263, doi:10.1007/BF00624353.

Thordarson, T., and S. Self (1996), Sulfur, chlorine and fluorine degassing and atmospheric loading by the Roza eruption, Columbia River Basalt Group, Washington, USA, *J. Volcanol. Geotherm. Res.*, *74*, 49–73, doi:10.1016/S0377-0273(96)00054-6.

Thornhill, G. D. (1993), Theoretical modeling of eruption plumes on Venus, *J. Geophys. Res.*, *98*(E5), 9107–9111, doi:10.1029/93JE00255.

Walker, G. P. L., S. Self, and L. Wilson (1984), Tarawera 1886, New Zealand: A basaltic plinian fissure eruption, *J. Volcanol. Geotherm. Res.*, *21*, 61–78, doi:10.1016/0377-0273(84)90016-7.

Wallace, J. M., and P. V. Hobbs (1977), *Atmospheric Science: An Introductory Survey*, 467 pp., Academic, Orlando, Fla.

Wilson, L. (1976), Explosive volcanic eruptions-III. Plinian eruption columns, *J. R. Astron. Soc.*, *45*, 543–556.

Wilson, L., and J. W. Head (2007), Explosive volcanic eruptions on Mars: Tephra and accretionary lapilli formation, dispersal and recognition in the geologic record, *J. Volcanol. Geotherm. Res.*, *163*, 83–97, doi:10.1016/j.jvolgeores.2007.03.007.

Wilson, L., and P. J. Mouginis-Mark (2001), Estimation of volcanic eruption conditions for a large flank event on Elysium Mons, Mars, *J. Geophys. Res.*, *106*(E9), 20,621–20,628, doi:10.1029/2000JE001420.

Wilson, L., R. S. J. Sparks, T. C. Huang, and N. D. Watkins (1978), The control of volcanic column heights by eruption energetics and dynamics, *J. Geophys. Res.*, *83*(B4), 1829–1836, doi:10.1029/JB083iB04p01829.

Woods, A. W. (1988), The fluid dynamics and thermodynamics of eruption columns, *Bull. Volcanol.*, *50*, 169–193, doi:10.1007/BF01079681.

Woods, A. W. (1993a), A model of the plumes above basaltic fissure eruptions, *Geophys. Res. Lett.*, *20*(12), 1115–1118, doi:10.1029/93GL01215.

Woods, A. W. (1993b), Moist convection and the injection of volcanic ash into the atmosphere, *J. Geophys. Res.*, *98*(B10), 17,627–17,636, doi:10.1029/93JB00718.

S. M. Baloga, Proxemy Research, 20528 Farcroft Ln., Gaithersburg, MD 20882, USA. (Steve@Proxemy.com)

L. S. Glaze, NASA Goddard Space Flight Center, Greenbelt, MD 20771, USA. (Lori.S.Glaze@nasa.gov)

J. Wimert, Department of Geology, University of Maryland, College Park, MD 20742, USA. (jwimert@umd.edu)